Phosphatidylserine and FVa Regulate FXa Structure

Kinshuk Raj Srivasatava[1], **Rinku Majumder**[1], **William H. Kane**[2], **Mary Ann Quinn-Allen**[3], and **Barry R Lentz**[1]

[1]Department of Biochemistry & Biophysics and Program in Molecular & Cellular Biophysics; University of North Carolina, Chapel Hill, NC 27599-7260

[2]Formerly of the Division of Hematology, Departments of Medicine and Pathology, Duke University Medical Center, Durham, NC 27710

[3]Mary Ann Quinn-Allen, BSMT (ASCP), Dept. of Molecular Pathology, Duke University Health System, Durham, NC 2771

Abstract

Human coagulation factor Xa (FXa) plays a key role in blood coagulation by activating prothrombin to thrombin on "stimulated" platelet membranes in the presence of its cofactor factor Va (FVa). Phosphatidylserine (PS) exposure on activated platelet membranes promotes prothrombin activation by FXa by allosterically regulating FXa. To identify the structural basis of this allosteric regulation, we used fluorescence resonance energy transfer (FRET) to monitor changes in FXa length in response 1] to soluble PS (dicaproyl-phosphatidylserine; C6PS), 2] to PS membranes, and 3] to FVa in the presence of C6PS and membranes. We incorporated a FRET pair with donor (fluorescein) at the active site and acceptor (Alexa fluor 555) at FXa N-terminus near the membrane. The results demonstrated that FXa structure changes upon binding of C6PS to two sites, a regulatory site (Reg site) at the N-terminus (previously identified as involving the Gla and EGF_N domains) and a presumptive protein-recognition site in the catalytic domain (Prot site). Binding of C6PS to the regulatory site increased the inter-probe distance by ~ 3 Å, while saturation of both sites further increased the distance by ~ 6.4 Å. FXa binding to a membrane produced a smaller length increase (~1.4 Å), indicating that FXa has a somewhat different structure on a membrane than when bound to C6PS in solution. However, when both FVa_2 (a FVa glycoform) and either C6PS or PS-containing membranes bound to FXa, the overall change in length was comparable (~ 5.6–5.8 Å), indicating that C6PS and PS-containing membranes in conjunction with FVa_2 have comparable regulatory effects on FXa. We conclude that the similar functional regulation of FXa by C6PS or membranes in conjunction with FVa_2 correlates with similar structural regulation. The results demonstrate the usefulness of FRET in analyzing structure-function relationships in FXa and in the $FXa.FVa_2$ complex.

Introduction

Prothrombinase complex plays a central role in blood coagulation by producing thrombin[1]. In assembling the prothrombinase complex, the enzyme FXa binds to its cofactor FVa and substrate prothrombin on activated platelet membranes in the presence of Ca^{2+} ions [2,3]. Appearance of phosphatidylserine (PS) on the surface of activated platelets is essential for assembly of fully active prothrombinase complex [4,5]. Extensive studies using a soluble form of PS (dicaproyl PS, C6PS) have shown that C6PS binds to single regulatory sites in both FXa and in a FVa glycoform [6] (FVa_2) to control both activity and assembly of a $FXa·FVa_2$ complex in solution[7–12], as does membrane-located PS[10,13]. Because the regulatory sites in both proteins are near the membrane binding regions and far from the "action ends" of these proteins (active site of FXa, FXa and binding region of FVa), PS is an allosteric regulator of both proteins [10,12]. While models of allostery differ, most can be interpreted in terms of a shift in average conformational state of a protein upon binding of the regulator. While FXa secondary structure and intrinsic fluorescence are altered by C6PS binding [14], still unknown is how the overall shape of FXa is altered by PS binding. This issue is particularly relevant because FXa has three flexible regions that join its four principle domains. Our hypothesis is that information from binding of PS to the N-terminus travels from the regulatory site near the membrane-binding domains (Gla and EGFn)[12] to the catalytic domain *via* changes in the flexible regions that connect Gla to EGFn, EGFn to EGFc, and EGFc to the catalytic domain. If so, we expect to see measurable changes in the shape of the molecule as reported for prothrombin when it interacts with membranes containing PS[15].

FXa has two chains and four domains(16). The light chain consists of three domains (Gla-EGF_N-EGF_C), which are joined by a disulfide linkage to the heavy chain catalytic domain. FXa is produced from its zymogen form (FX) by proteolytic cleavage of a peptide bond (Arg194-Ile195 in the chymotrypsin numbering system), resulting in release of an activation peptide from the N-terminus of the catalytic domain. A decent molecular model for FXa has been proposed based on crystal structures and all atom molecular dynamics simulations [17]. This model places the active site roughly 8.3 nm from a plane of Ca^{2+} ions that are presumed to sit at the membrane interface, while the corresponding distance in the inactive zymogen is predicted to be 9.5 nm. Two fluorescence resonance transfer experiments report the distance between active site-located probes and membrane-located probes [18,19], although these estimates differed by more than 2 nm. There are several studies, both FRET-based [18–20] and computation-based [21], that purport to show a change in FXa structure upon binding factor Va. All FRET-based measurements reflect changes in distances between the FXa active site and a membrane surface. A change in this distance can result from conformational changes or from a change in the orientation of FXa relative to the membrane surface. The phosphatidylserine (PS) binding site that regulates FXa conformation and

activity [8,9,14] is located in the Gla and EGF_N domains [12], although membrane binding is widely viewed as mediated by the Gla domain [22]. Thus, it is conceivable that FXa orients on the membrane surface so that both the plane of Ca^{2+} ions within the Gla domain and its neighboring EGF_N/Gla interface lie close to the plane of the membrane. This would require considerable reorientation in the flexible regions of the EGF_N and EGF_C domains relative to the orientation seen in the current model for FXa structure [17]. These interpretations can be resolved by placing fluorescent probes at two locations within the FXa molecule, as we do in this report. In addition, using a soluble short chain PS molecule (dicaproyl PS: C6PS), we ask whether interaction with a PS-containing membrane is required to trigger FXa conformational changes or whether occupancy of the PS-specific regulatory site on FXa is sufficient. Finally, we ask whether interaction with factor Va triggers conformational changes in FXa or simply reorients FXa relative to the membrane surface.

In order to answer these questions, we investigated C6PS binding and its effect on the structure of FXa by monitoring changes in intramolecular FRET signals. To do so, we incorporated an appropriate donor-acceptor fluorophore pair in two regions of FXa separated by a distance estimated to be roughly 70–90 Å based on a current structural model of FXa structure [17]. We recorded the fluorescence intensity of donor-labeled, acceptor-labeled, and donor and acceptor in double-labeled FXa with increasing concentrations of C6PS. We then calculated E_{FRET} and inter-probe distance as a function of C6PS concentration. The results confirmed the existence of two sites in FXa whose occupancy significantly lengthens its structure (~9.4 Å out of 80 Å) upon saturation with C6PS, with the regulatory site being near the N-terminus and a second linked binding site near the active site [12]. Significantly, addition of FVa after occupancy of the regulatory site further lengthened FXa, but not by the same amount as addition of FVa after occupancy of the second site, supporting our previous hypothesis that the second site is anomalous and part of recognition site(s) for one or more proteins[12]. Also of interest, binding of FXa to a PS-containing membrane produced a smaller conformational change than seen with C6PS, indicating that the interaction of the Gla domain with the membrane surface also plays a role in modulating FXa structure. Overall, our results demonstrate a heretofore unrecognized and complex regulation of FXa structure by PS, FVa, and a membrane surface.

Experimental Procedures

Materials

Human Factor X_a, prothrombin, Factor X activator from Russell's viper venom (RVV-X) and Fluorescein-labeled EGR-chloromethylketone (FEGRck) were purchased from Haematologic Technologies Inc. (Essex Juction, VT). The chromogenic substrates S2765 and S2238 were purchased from Chromogenix (Bedford, MA, USA). Recombinant human factor Va (FVa_2) with a N2181Q mutation [6] was expressed in a BHK cell line kindly provided by Dr. Rodney Camire (Children's Hospital of the University of Pennsylvania). The factor V NQ (N2181Q) des B DNA was subcloned into the pED vector obtained from Wyeth Laboratories (Collegeville, PA, USA) (the NQ mutation eliminates an N-glycosylation site at Asn-2181 that is partially glycosylated *in vivo*, with the un-glycosylated

form binding significantly more tightly to FXa in the presence of C6PS[6]. Co-transfection of the pED FV with psV2Neo into BHK-M cells was followed by selection with G418, resulting in stable transfection of rHFV NQ des B with a typical yield of ~4–10 mcg/mL. FVa_2 was first concentrated on SP Sepharose, then thrombin-activated and purified over Mono S HR 5/5 anion-exchange column as previously described[6], yielding milligram quantities of fully active, ~95% pure FVa_2 (the form of the protein lacking the oligosaccharide at position 2181). The activity of FVa_2 was assayed using 25:75 DOPS:DOPC vesicles or C6PS as previously described[11]. Alexa Fluor 555 carboxylic acid, succinimidyl ester was purchased from Invitrogen Molecular Probes. 1,2-dihexanoyl-sn-glycero-3-phospho-L-serine (sodium salt) (C6PS) and 1,2 dioleoyl - 3sn-phosphatidylcholine (DOPC) and 1,2-dioleoyl-sn-glycero-3-phospho-L-serine (sodium salt) (DOPS) were purchased from Avanti polar Lipids (Birmingham, AL, USA). PD-10 desalting and HiTrap QFF columns were purchased from GE Healthcare Life Sciences. All other chemicals were ACS reagent grade and solvents were of HPLC grade, purchased from Fisher Scientific and Sigma Aldrich.

Methods

Design and Preparation of Single and Double Fluorescent Labeled FXa—To examine conformational change associated with C6PS binding, we measured intramolecular FRET between a donor-acceptor pair incorporated into FXa. Our hypothesis was that flexible regions between the Gla, EGFn, EGFc, and catalytic domains are important in transmitting information between the regulatory PS binding site in the Gla-EGFn domains and the apparently anomalous C6PS binding site in the catalytic domain[12]. Thus, we incorporated one fluorophore at the N-terminus (Gla domain) and another in the catalytic domain. We incorporated the donor (fluorescein) in the active site using Fluorescein-EGRck and the acceptor (Alexa fluor 555) using succinimidyl ester chemistry to label the N-terminal primary amine. The efficiency of FRET depends upon optimal spectral overlap between donor emission and acceptor absorption and on the distance between fluorophores. A wide variety of FRET pairs with appropriate spectral overlap have been identified, but one must choose an appropriate pair for the distance to be measured. Thus, we chose the Fluorescein-Alexa Fluor 555 pair (Förster distance = R_0 = 7 nm) for our study based on their spectral properties and the reported distance (89 Å, [17]) between their sites of attachment in FXa.

The overall design of labeled FXa species and the paths taken to achieve them are given in Scheme 1. We first labeled the N-terminal primary amines of FX by incubating overnight at 4 °C with a 50-fold molar excess of Alexa555 succinimidyl ester in a buffer consisting of 0.1 M sodium phosphate, 150 mM NaCl at pH 7.2. Selective labeling of proteins at their N-termini is routinely accomplished at pH 7.2 using succinimidyl esters. The N-terminal α-amino group pKa (8.9) is considerably lower than that of the lysine ε-amino group (pKa = 10.5); thus, at pH 7.2 lysine amines are very rarely in the unprotonated state (probability ~ 0.1%) and remain unreactive towards succinimidyl esters. Since FXa has only 12 exposed lysines [23], the probability of labeling a Lys in a FXa under our conditions would be only ~ 0.01, too small to significantly influence our interpretation of FRET results. FX consists of two peptide chains connected by a disulfide linkage; both N-termini will react with

Alexa555 succinimidyl ester, yielding a double-labeled FX. Following labeling, the unreacted dye was removed by extensive dialysis at 4 °C. The N-terminal-labeled FX was then activated by incubating it with RVV-X (1: 100 RVV/X stoichiometry) at 37 °C for 1 hour in 50 mM Tris, 150 mM NaCl, 5 mM CaCl$_2$, 0.6 % PEG, pH 7.4. This reaction removes the catalytic domain N-terminal activation peptide, leaving FXa with acceptor A555 only at the Gla-domain N-terminus. Amidolytic activity during RVV treatment was measured using the synthetic substrate S2765, whose absorbance was recorded at 405 nm using a tunable microplate reader (Versamax; Molecular Device Corp., Sunnyvale, CA). The Gla-labeled FXa was fully active by this measure. N-terminal Alexa fluor 555-labeled FXa was purified from RVV and cleaved activation peptide using a Hi-Trap anion exchange column mounted on a AKTA FPLC instrument (GE Health Care). N-terminal labeled FXa eluted at ~ 0.4–0.45 M NaCl. Purity of the labeled FXa was confirmed by fluoroimaging on a Typhoon Trio$^+$ variable mode Imager (GE Health Care) followed by Coomassie staining of the SDS PAGE gel.

To prepare double-labeled FXa, we then reacted N-terminal-labeled FXa with FEGRck, which attaches fluorescein to the active site *via* the peptide EGR chemically linked to the active site histidine. FXa was incubated with a 10-fold molar excess of FEGRck in 50 mM Tris, 150 mM NaCl, 5 mM CaCl$_2$, 0.6 % PEG, pH 7.4 at 24°C for 2.5 hour in the dark. The progress of active site labeling was monitored using the synthetic substrate S2765, with complete loss of amidolytic activity indicating complete labeling. Unreacted FEGRck was removed by extensive dialysis at 4 °C with followed by gel filtration on a PD-10 desalting column.

The extent of fluorescence labeling was determined as described by Bock[24]. We used molar extinction coefficients of 155,000 M^{-1} cm^{-1} at 555 nm for Alexa fluor 555 and 84000 M^{-1} cm^{-1} at 495 nm for fluorescein. In estimating fluorophore concentration, we used methods and correction factors of 0.08 for Alexa fluor 555 and of 0.19 for fluorescein (from Invitrogen) to correct for the contribution of the dye to 280 nm absorbance. The extent of labeling was 0.5 for the N-terminal Alexa acceptor and 0.85 for the active-site-located donor fluorescein, whether alone or in FXa already labeled with acceptor. Only acceptor extent of labeling (f_a) is used to correct FRET efficiency.

Preparation of Phospholipid Vesicles—The concentrations of di-oleoyl-phosphatidylcholine (DOPC) and di-oleoyl-phosphatidylserine (DOPS) stock solutions in chloroform were determined by micro-phosphate assay [25]. The DOPC stock was "spiked" with ^{14}C-dipalmitoyl phosphatidylcholine (0.01 mol fraction) and its specific activity determined by scintillation counting. Lipid stock solutions were mixed to obtain a stock containing 75% DOPC (^{14}C, radiolabeled) and 25% DOPS in chloroform. Appropriate volumes of this solution were removed for each experiment and placed in 1 mL amber vials from which a stream of nitrogen evaporated the chloroform. Thereafter, the lipid mixture was re-dissolved in cyclohexane and a few drops of methanol and then frozen and lyophilized to a white powder. To prepare small unilamellar vesicles (SUVs), the lyophilized DOPC/DOPS powder was suspended by vigorous vortexing in 2 mL of Tris buffer (20 mM Tris, 150 mM NaCl, pH 7.4). The lipid suspension was transferred to an annealed glass vial and sonicated using a titanium tip with a Misonix Sonicator 3000. SUVs

were isolated via centrifugation at 70,000 rpm at 4 °C for 25 minutes in a Beckman TL-100 ultracentrifuge. SUV concentration was determined using ^{14}C scintillation counting.

Critical Micelle Concentration Measurements—C6PS CMCs were determined as described previously and as is now routine in our lab [11]. No results are presented for C6PS concentrations above the measured CMC.

Fluorescence Measurements

Steady state fluorescence and anisotropy measurements were performed in 50 mM Tris, 150 mM NaCl, 5 mM CaCl2, 0.6% PEG, 7.4 pH upon titration with C6PS at 23°C with a FluoroMax-4 spectrofluorometer (Horiba Jobin Yvon Inc., Edison, NJ). Intensity and anisotropy were recorded using 4 nm bandwidths for both excitation and emission monochromators with excitation at 495 nm for fluorescein and at 551 nm for Alexa 555 and emission wavelengths of 520 nm and 565 nm, respectively. The excitation shutter was closed except during data collection to limit photo-degradation. Fluorescence experiments were performed in 1 mL quartz cuvettes preconditioned with 50 nM unlabeled FXa protein in buffer. After the incubation, the cuvette was thrice rinsed with buffer before adding the labeled FXa. Anisotropies of labeled FXa were recorded in buffer alone and on addition of both C6PS and phospholipid vesicles separately. Fluorescence intensities were recorded with increasing concentration of C6PS and the observed fluorescence intensities were corrected for dilution. A maximum of 10 μL phospholipid vesicles was added per experiment. Measurements were taken ~3 min after each addition, with values averaged to obtain a mean and standard deviation. Fluorescence intensities were normalized against the intensities of reference samples (aqueous solutions of Alexa Fluor 555 carboxylic acid, succinimidyl ester or of FEGRck and were averaged both within and between experiments (at least 6 points per value).

Analysis of FRET Data

We calculated FRET efficiency (E_{FRET}) corresponding to each averaged fluorescence intensity measurement using equation 1[26]:

$$E = \left(1 - \frac{F_{DA}}{F_D}\right)\left(\frac{1}{f_a}\right) \quad (1)$$

F_{DA} is the fluorescence intensity of donor when acceptor is present in double-labeled FXa, and F_D is the fluorescence intensity of donor-labeled FXa. The apparent fluorescent intensities were corrected using labeling efficiency of the acceptor (f_a), *i.e.*, the average number of acceptor dye molecules attached per protein (0.5). The distance between the donor and acceptor dyes (R) was obtained as:

$$R = R_o\left(\frac{1}{E} - 1\right)^{1/6} \quad (2)$$

We used 70 Å for the Förster radius (R_0) of the fluorescein-Alexa fluor 555 pair, as provided by the manufacturer (Invitrogen). FRET efficiency is affected by the distance between fluorophores and by the relative orientation of donor and acceptor dipoles, as expressed in the orientation factor κ^2 [26]. Reported R_0 values normally assume $\kappa^2 = 2/3$, which implies random orientation of donor emission and acceptor excitation dipoles. This assumption produces "$R_{2/3}$" from equation 2, namely an estimate of inter-probe distance that depends on the assumption that the orientational factor corresponds to random relative orientation. This approach is acceptable for estimating changes in R as long as the orientation factor is not expected to change significantly with whatever conformational change leads to a change in R. To obtain estimates of absolute distances, one must estimate the uncertainty in R associated with the uncertainty in κ^2. The fluorescence anisotropies of fluorophores in single-labeled FXa were recorded using the respective excitation and emission wavelengths for fluorescein in donor-labeled FXa and for Alexa fluor 555 in acceptor-labeled FXa. The anisotropies of fluorescein and Alexa-labeled FXa were recorded in buffer alone, and then under all conditions where E_{FRET} was obtained from experimental intensities. Based on theses fluorescence anisotropy measurements and using reported values of the intrinsic anisotropies (0.4) (r_0) of both dyes[27,28], we calculated relative anisotropies ($d_i^x = (r_i/r_0)$) and estimated the range of possible κ^2 values (κ^2_{min} to κ^2_{max}) according to equations 3 and 4[29].

$$\kappa^2_{\min} = \frac{2}{3}\left[1 - \left(\frac{d_D^x + d_A^x}{2}\right)\right] \quad (3)$$

$$\kappa^2_{\max} = \frac{2}{3}\left(1 + d_D^x + d_A^x + 3d_D^x d_A^x\right) \quad (4)$$

Using this range of κ^2, we calculated the range of distances between donor and acceptor fluorophore covalently attached to amino acid residues of FXa:

$$R_{\min} = \left(\frac{\kappa^2_{\min}}{(2/3)}\right)^{1/6} R_{2/3} \quad (5)$$

$$R_{\max} = \left(\frac{\kappa^2_{\max}}{(2/3)}\right)^{1/6} R_{2/3} \quad (6)$$

Because r (thus, κ^2) of donor and acceptor varied with increasing C6PS concentration, we report a range of values for R and a mean of that range (Table 1). By comparing $R_{2/3}$ with these mean values, we see discrepancies of ~ 2.5 Å. However, the same Table shows that changes associated with addition of C6PS generally differed by less than 0.5 Å when obtained by these two methods. Therefore, we used $R_{2/3}$ for C6PS and membrane titrations to obtain R in most instances, and calculated ranges of R values in only certain instances to estimate what the maximal errors in absolute distances might be.

Fitting C6PS Titration Data—Because we know that FXa has two C6PS binding sites [12,14], we analyzed our titration data according to different models that account for one or two binding sites. The data in Figure 2B suggested a model in which two linked sites are occupied sequentially. We considered both a single-site binding model and a linked-site, sequential binding model.

$$\text{Single Site:} F_{obs} = F_0 + \Delta F \left(\frac{K_1[C6PS]}{1 + K_1[C6PS]} \right) \quad (7)$$

Here, F_{obs} is the observed fluorescence at any C6PS concentration, K_1 is the site association constant, F_0 is the fluorescence intensity in the absence of C6PS (*i.e.*, with the site unoccupied), and F is the fluorescence intensity change from occupying this site.

$$\text{Linked, sequential:} F_{obs} = F_0 / \Theta + F_1 \left(\frac{K_1[C6PS]}{\Theta} \right) + F_{12} \left(\frac{K_1 K_2[C6PS]^2}{\Theta} \right); \Theta$$
$$= 1 + K_1[C6PS]$$
$$+ K_1 K_{12}[C6PS]^2 \quad (8)$$

Again, F_{obs} is the observed fluorescence at any C6PS concentration, K_1 is the site association constant for site 1; F_0 is the fluorescence intensity in the absence of C6PS; F_1 is the intensity of the species with site 1 occupied, and F_{12} is the intensity of the species with both sites occupied; and K_1 and K_{12} are the site binding constants for sequential occupancy of sites 1 and 2, respectively. We use [C6PS]$_{\text{free}} \simeq$ [C6PS]$_{\text{tot}}$ = [C6PS] in these expressions because the concentration of C6PS is much greater than that of FXa. SigmaPlot (Version 10.0 for windows, Jandel Scientific) was used for non-linear regression analysis. The appropriateness of a fit was judged by the coefficient of determination R^2 and F-statistics with a P-value test.

Results

Soluble C6PS binding to FXa

We recorded the fluorescence intensity of donor-labeled (F_D), acceptor-labeled (F_A), and donor (F_{DA}) and acceptor (F_{AD}) in double-labeled FXa upon titration with C6PS. Results are presented in Figures 1 and 2. The fluorescence intensity of both donor and acceptor decreased with increasing C6PS concentration. Addition of buffer alone led to a trivially small decrees in intensity due to dilution effects, so the drop in fluorescence intensity was due either to quenching by minor impurities in C6PS stocks, but much more likely to conformational changes in FXa induced by PS binding. The results for both F_A (Figure 1A) and F_{AD} (Figure 2A) were consistent with a single-site binding model (Equation S7) with saturation at ~200–300 µM C6PS and K_d value 73 ± 8 µM for F_A and 67 ± 6 µM for F_{AD}, consistent with reports for binding of C6PS mainly to the regulatory site in the Gla-EGFn domains[12] with K_d estimated to be 73–90 µM[7,9,14]. It appears that the acceptor probe present at the N-terminus is sensitive only to binding to the regulatory site (termed site "Reg"), which follows a simple single-site model.

The fluorescence from the donor fluorescein at the active site behaved differently. The curves for F_{DA} (Figure 2B) and F_D (Figure 1B) did not fully saturate by 700 μM C6PS, above which micelles form. Application of a single-site binding model to these data gave 333 ± 34 μM for F_D and 370 ± 54 μM for F_{DA} (Figures 1B and 2B, dotted curves). The residuals for the single-binding-site model were still within error estimates but appeared to be non-random, especially for F_{DA} in the range of 0 to 300 μM C6PS (Figure 2B). In this case, the curve clearly showed evidence of two events, the first with a tight K_d (~ 56 μM) saturating around 200 μM C6PS, and the second with a large K_d showing no sign of saturating (Figure 2B). Thus, the donor probe in the catalytic domain reports binding to the low affinity site in this domain[14] but appears to be sensitive to binding of C6PS to the tight N-terminal regulatory site as well. Previous studies have reported that FXa labeled at its active site with a different fluorescent probe (Dansyl; DEGR-Xa) bound C6PS according to a two-linked-site, sequential binding model, a conclusion made possible by C6PS triggering fluorescence changes of opposite signs upon occupying the two sites [14]. In the case of FEGR-Xa, we apparently did not have this lucky situation, so the data were less useful in defining all four parameters needed to define the two-linked-site, sequential binding model (K_1, K_{12}, F_1, and F_{12}, Equation 8). Nonetheless, the F_{DA} data indicate that binding to the tight site in the regulatory domain triggers changes in the distance between the probes in the regulatory and active site regions. Because of this and because the F_{DA} data appeared to have a greater indication of two-site binding, we focused first on this data set. We initially tried fixing K_1 at 73 μM, but variation of K_{12}, F_1, and F_{12} could not produce the curvature in the data seen at low C6PS concentration (0–150 μM). We next fixed F_1 at the apparent plateau in the F_{DA} data from 140–175 μM C6PS (0.804; Figure 2B) and fixed F_{12} based on the first round of χ^2 minimization (714 μM), and then varied K_1 and F_{12} to obtain K_{d1} = 56 μM and F_{12} = 0.694. This adjustment led to a slightly better fit in the low C6PS region but still not significantly better than a single-site model. Next, we allowed F_{12} and K_{12} to vary with K_{d1} = 56 μM and F_1 = 0.804 fixed to obtain new estimates of K_{12} ($K_{d12} \approx 1000$μM, F_{12} = 0.657). This approach improved the fit above 200 μM C6PS without significantly degrading it below 175 μM. Finally, we re-optimized K_1 with all other parameters fixed to obtain K_{d1} = 50 ± 12 μM and significantly better residuals than obtained with a single-site model over the range of C6PS concentration from 0 to 120 μM (Figure 2B). The only way to improve the fit between 0 and 120 μM was to allow both K_1 and F_1 to vary and optimize to physically unreasonable values (K_{d1} = 15 μM, F_1 = 0.813). We conclude that, while a sequential, linked-site model offers a slightly better description of the F_{DA} data at both low (< 100 μM) and middle range (200–400 μM) C6PS concentrations, such a model still provides an incomplete description of the data in the range of 175–250 μM C6PS. Either there may be more than two sites or the linked, sequential binding model is inappropriate. Because the former is proven untrue by equilibrium dialysis experiments [12], we conclude that linkage between the weak site ("Prot" site) and the tight site ("Reg" site) is likely more complex than we can discern from our data. Our previous analysis of C6PS binding to FXa suggested both such linkage, but ultimately required explanation in terms of dimer formation *via* interactions between the catalytic domains of two FXa molecules [14,23]. This could be a likely explanation for our imperfect description of F_{DA}.

Next, we attempted to describe the F_D data analytically. Application of the single-site model produced the dotted curve in Figure 1B with the residuals shown below the data, with $k_d = 333 \pm 34$ and $F_{sat} = 0.20 \pm 0.010$. As is evident, the residuals from the single-site model were within acceptable limits and showed limited persistence except at high C6PS concentrations. However, this K_d is not what we obtain from the F_{DA} results for either K_{d1} or K_{d12}, but is in between these values. Based on these observations, it was clear that the F_D data alone would not permit estimation of the critical parameters required for describing this data set (F_1, F_{12}, K_{d1} and K_{d12}). Thus, we asked whether we could reasonably describe the F_D data by a two-linked-site sequential binding model (Equation 8) using binding constants that offered the best description of the F_{DA} data so as to obtain F_1 and F_{12} estimates consistent with the analysis of the F_{DA} data. Again, we followed an iterative procedure similar to that described for the F_{DA} data to determine whether a sequential, two-linked site model might improve the description of the F_D data. We first adjusted F_{12} with K_{d1} and K_{d12} fixed at values based on fitting F_{DA} (53 μM and 714 μM), and F_1 (0.946) based on visual examination of the data. We next varied both F_1 and F_{12} to obtain new estimates of these parameters with K_1 and K_{12} fixed as above. Then, we used a very weak value of K_{d12} as obtained from F_{DA} analysis (1000 μM), and found that only F_{12} (not the experimentally estimated value of F_1) was sensitive to the value of K_{d12}. We next fixed K_{d12} at its initial value (714 μM) and K_{d1} at the value 73 μM reported previously [9] to conclude that the optimal F_1 was not sensitive to K_{d12}. With this information, we fixed F_1 (0.946), F_{12} (0.7697) and optimized K_{d1} to obtain 68 μM. This estimate of k_{d1} was then fixed and K_{12} and F_{12} re-optimized to obtain $K_{d12} = 769$ μM and $F_{12} = 0.758$, respectively. Although the F_D and F_{DA} data contained insufficient information to precisely define the Reg and Prot site binding constants (K_1 and K_{12}), we showed in this way that analyses of both sets of data according to the two-linked-site sequential model were consistent with a fairly tight Reg site in the regulatory region ($k_{d1} \sim$ 56–73 μM) and a weak linked site in the catalytic site region (Prot site, $k_{d12} \sim$ 770 – 1100 μM). These values agree with previous estimates: $K_{d1} \sim 73$ μM [9] and $K_{d1} \sim 90$ μM with $K_{d12} \sim$ 255–1400 μM [14]. We conclude that, while the F_D data cannot define values of K_{d1} and K_{d12}, the F_D data are consistent with binding constants estimated from F_A, F_{DA}, and F_{AD} curves and with values reported previously [9,14]. This result provided the F_1 and F_{12} values from both F_{DA} and F_D measurements to calculate FRET efficiencies and to estimate changes in inter-probe distances upon binding of C6PS to the Reg (F_1) or Prot (F_{12}) sites. We address this estimate in the Discussion.

Energy Transfer Efficiency

The efficiency of energy transfer (E_{FRET}) was calculated from experimental F_{DA} and F_D values using Equation 1 at each C6PS concentration. These efficiencies are plotted against C6PS concentration in Figure 3. The biphasic behavior that was obvious in F_{DA} is clearly not as evident in E_{FRET} because it is not evident in the F_D titration, and E_{FRET} is obtained by taking the ratio of F_{DA} over F_D (Equation 1). However, there is not the clear, non-random distribution of residuals at low C6PS concentration that we saw especially for F_{DA} but to some extent for F_D. There remains only the peak in residuals at roughly 220 μM that was present in both F_D and F_{DA} fits in the range of 175–250 μM. Because the abilities of single-site or two-linked sequential-sites models were barely indistinguishable in describing these data, this left uncertainty as to how best to determine E_{FRET} for the two states defined by

occupying the two C6PS sites on FXa. We used two procedures. First, we reasoned that saturation of the regulatory site (site 1) was likely occurring in the range of C6PS concentrations for which residuals were maximal, roughly 175–250 µM for both F_{DA} and F_D, with at 200 µM C6PS actually used to calculate $E_{FRET,1}$. A second, and more straightforward approach was to use F_1 values obtained from fitting the F_{DA} and F_D titration curves to the sequential, two-site model to obtain E_{FRET} for site 1. The values of $R_{2/3,R}$ (the change in inter-probe distance for occupation of the regulatory site) by these two methods were –0.057 and –0.052, respectively. We again considered two methods to estimate the E_{FRET} (and thus R) associated with occupying the second C6PS site in FXa. The first was to simply use F_D and F_{DA} for the highest C6PS concentration accessible (700 µM), above which C6PS forms micelles under our experimental conditions. The R_P values obtained at 700 µM C6PS were 5.8 Å by the $\kappa^2 = 2/3$ method *versus* 5.2 Å by the κ^2- range method. The second and again most direct method was to use F_{12} from fitting F_{DA} and F_D titrations to the sequential, two-component binding model. The final saturation obtained by the second method R_P was quite large (9Å by the κ^2-range method and 9.4Å by the $R_{2/3}$ method). Values from different methods are compared in Table 1's fourth and fifth rows. From this, we judge that the second C6PS site is quite weak and is not saturated even at the highest C6PS concentrations experimentally accessible.

As noted, uncertainty in κ^2 affected our estimates of R. κ^2 factors can be estimated from relative fluorescence anisotropies of the two probes involved in the FRET pair [29] (see Equations 3–6). Fluorescence anisotropies of donor (r_D) and acceptor (r_A) were recorded for FXa in the three states of C6PS occupation considered here: FXa ($r_D = 0.17$; $r_A = 0.24$); FXa.C6PS ($r_D = 0.18$; $r_A = 0.27$); and of FXa.$(C6PS)_2$ ($r_D = 0.22$; $r_A = 0.29$). Minimal and maximal estimates of R obtained from Equations 4–6 are given in Table 1 along with the values obtained using κ^2 of 2/3. Comparing R values obtained using κ^2 of 2/3 with the mean of the range using proper κ^2 corrections (Tables 1 & 2), the R values with κ^2 of 2/3 were always about 2.5 Å smaller than the mean of those obtained using κ^2_{min} and κ^2_{max} from Equations 5 and 6. However, the changes in distances associated with going from state FXa to state FXa.C6PS (site Reg occupied) to state FXa.$(C6PS)_2$ (both Reg and Prot site occupied) were nearly the same (within 0.5 Å) for both methods of estimating R_R and R_P. The fact that distances calculated with a κ^2 of 2/3 were slightly smaller indicates that probe dipoles were somewhat favorably oriented in the FXa molecule. The fact that changes in R between states were not significantly influenced by the exact value of κ^2 means that the orientation effect was not significantly different in the different states. Thus, we use $R_{2/3}$ for further interpretations.

Factor Va Binding Replaces C6PS in the Weak or Prot Site

In FXa.$(C6PS)_2$, C6PS occupies the regulatory site (Reg site) in the EGFn-Gla domains and the anomalous site in the catalytic domain (Prot-site), which we have previously suggested might be a protein-binding site [12]. To test this suggestion, we performed experiments in which FVa_2 (final concentration 50 nM) was added to FXa (15 nM) following a 3-minute incubation with increasing concentrations of C6PS. After an initial incubation with 200 µM C6PS to form FXa.C6PS, we added FVa_2 and incubated for 3 minutes to assemble the C6PS.FVa_2.FXa.C6PS complex. Tightly associated FVa and FXa serve as the essential

prothrombin-activating complex that assembles on PS-containing platelet membranes. We have shown previously that C6PS triggers assembly of this complex in solution [11,30]. Human FVa_2 binds C6PS to its regulatory domain (C1) with a $K_{d,app}$ of 4 nM [10], and then binds FXa with a K_d of 0.6 nM [11]. Thus, FVa_2's regulatory site will be saturated with the C6PS under our experimental conditions. We calculated the E_{FRET} from the intensities of F_D and F_{DA} before and after addition of FVa_2 in the presence of C6PS. The results are displayed in Figure 4. We continued this process until we reached the highest C6PS concentration for which C6PS does not form micelles under these conditions (700 μM). It is clear that FVa_2 and C6PS increased the inter-probe distance by ~ 5.8 Å, 3 Å more than the 2.8 Å resulting from formation of state FXa.C6PS but comparable to that estimated for FXa. $(C6PS)_2$ at 700 μM C6PS (5.7 Å, Figure 3). These experiments were repeated with a different FXa preparation to yield 2.7 Å for FXa.C6PS and 5.6Å for $C6PS.FVa_2.FXa.C6PS$. Interestingly, this change was still much less than the ~ 9.4 Å change estimated for formation of the fully saturated $FXa.(C6PS)_2$ state (Table 1), making it clear that the $C6PS.FVa_2.FXa.C6PS$ state is distinct from the $FXa.(C6PS)_2$ state. The fact that the $C6PS.FVa_2.FXa.C6PS$ state completely supplanted the $FXa.(C6PS)_2$ at all C6PS concentrations above 200 μM (compare Figures 3 and 4) indicates that $C6PS.FVa_2.FXa.C6PS$ competes successfully with $FXa.(C6PS)_2$ and supports our hypothesis that weak binding of C6PS is anomalous and involves a protein-binding site.

Membrane-Association of FXa and formation of a membrane-Associated FVa-FXa Complex

We executed FRET experiments with SUVs and FVa_2 to study the conformational changes on binding of FVa to membrane-associated FXa. We measured F_D and F_{DA} of 15 μM singly and doubly labeled FXa in Tris buffer (50mM Tris, 150mM NaCl, 5 mM $CaCl_2$, 7.4 pH) in the presence of 150 μM unlabeled FXa and in the presence and absence of 50 μM SUVs. The reason for the presence of a 10-fold excess of unlabeled FXa was to minimize the contribution from inter-molecular FRET between FXa in dimers on the membrane surface, where dimerization is fairly extensive at 5 mM Ca^{2+} [31]. The recorded F_D and F_{DA} values were used to calculate E_{FRET} and corresponding inter-probe distances (assuming $\kappa^2 = 2/3$) as recorded in Table 2. The results indicate that the donor-acceptor distance increases by ~1.4 Å when FXa binds to a PS/PC membrane, a smaller distance than the 2.5 – 2.8 Å we observed when C6PS bound to FXa (Table 1). This distance increased by another ~ 4.6 Å upon binding of FVa_2 to membrane-associated FXa, for a total increase relative to FXa in solution of 6.0 Å. We also recorded the fluorescence anisotropy of FXa labeled with fluorescein in its active site (donor FXa). As seen in Table 2, this anisotropy was unaltered by binding of C6PS to form FXa.C6PS or even by binding of FXa to membranes. However, binding to FVa_2 in the presence of C6PS or membranes produced a significant increase in the anisotropy of fluorescein at the FXa active site. This result implies either a significant change in the rotational freedom of the probe attached to the active site or a change in the orientational freedom of the active site-bound EGR peptide. In either case, our results mean that FVa_2 binds to and alters the active site region and that this binding is linked to binding of C6PS to the regulatory region. Since many studies show that FVa binds to the FXa catalytic domain, our results confirm that Prot site is a protein-binding site in the catalytic domain that only anomalously responds to C6PS.

Discussion

The Reg-Site

Previous studies have suggested that up-regulation of FXa by C6PS is due to conformational changes induced by C6PS binding to two sites, but these reports did not provide direct evidence of large-scale changes in structure [7,12]. The acceptor probe (Alexa fluor 555) at the N-terminus responded to C6PS titration with a K_{d1} (~73 μM), making it clear that it monitored binding to the regulatory site previously shown to exist in the Gla-EGFn region [12] with a K_d in the range of 60–90 μM [7–9]. Our results reinforce the regulatory site's location and clearly show that FXa extends in length by ~ 2.8 Å (3.6%) upon occupancy of this site by C6PS. The uncertainties in our measured distance changes are much smaller (~0.7%) than this elongation, which thus constitutes a significant change in overall shape of the FXa molecule. We showed previously, using FRET, that FXa's substrates, prothrombin and meizothrombin (the active intermediate of prothrombin activation [3]), experience significant increases in length and/or changes in orientation on a membrane surface (+9% for meizothrombin and –22% for prothrombin) [15]. While the change in FXa's length upon occupancy of its Reg-site is much less than these changes, it is important to note that changes in prothrombin and meizothrombin are much less certain, both because they were measured with respect to a membrane-located probe and because the dimensions of the proteins in solution were estimated by hydrodynamics and not FRET. Nonetheless, the current results reinforce that PS (membrane-located or soluble C6PS) triggers significant conformational changes in both FXa and its substrates that are very likely associated with the 60-fold increase in k_{cat} [9] or with the shift in reaction path associated with membrane- [13] or C6PS- [7] binding to FXa.

The Prot-Site

The change in FXa structure upon saturation of the second C6PS site (Prot-site in the FXa catalytic domain [12]) was much greater (increase in donor-acceptor distance of ~6.4 Å or 8%) than that associated with occupying the Reg site (Tables 1 and 2). However, following occupancy of the Reg-site by C6PS, addition of FVa$_2$ produced an additional overall change in inter-probe distance (R, ~3 Å or 3.7%, Table 2) that was independent of the amount of C6PS added (Figure 4), but was considerably less than the extension produced by occupancy of the Prot site by C6PS. These observations suggest three conclusions: 1] the Prot-site is indeed a protein recognition site that is anomalously occupied at high C6PS concentration; 2] FVa$_2$ competes quite successfully with C6PS binding to this site; and 3] FVa binding to FXa with the regulatory site occupied (FXa.C6PS exists at 200 μM C6PS) elicits a substantial additional elongation (3 Å or 3.7%) in FXa beyond that associated with C6PS binding to the Reg-site. A significantly larger increase in R occurs when FVa$_2$ is added to FXa on a membrane (~ 4.6 Å or 5.8%, Table 2). Finally, we note that the change in inter-probe distance (R) is greater for saturation of both sites by C6PS (~9.4 Å, Tables 1) than it is for saturation of the R site by C6PS followed by FVa$_2$ binding (~5.8 Å, Table 2). The implications of these observations are discussed next.

Mechanistic Implications of Membrane-induced *versus* C6PS-induced Changes in the Presence and Absence of FVa$_2$

The kinetics of activation of prothrombin to its activation intermediates and then their further activation to thrombin are quite similar whether PS-containing membranes or C6PS are used to activate FXa [7,11]. Thus, we presumed that FXa would undergo similar structural changes upon binding to C6PS in solution as it does upon binding to PS-containing membranes. We found this presumption to be only qualitatively true (R ~ 1.4 Å for PS-containing membranes *versus* ~ 2.8 Å with C6PS; Tables 1 and 2). We suggest that this has to do with active-site-labeled FXa dimer formation on a membrane that does not occur when C6PS binds to FXa in solution [23,31]. Thus, our hypothesis is that FXa dimerization limits extension of FXa on a PS-containing membrane, but that FVa$_2$ binding to the catalytic domain competes with dimerization and extends the FXa molecule. This is consistent with the report that FXa dimerization competes with FVa$_2$ binding in solution [32] and with the observation that elongation caused by FVa$_2$ binding to FXa on a membrane is greater than observed for FXa whose Reg-site is occupied by C6PS. However, the membrane-assembled prothrombinase complex did show comparable FXa elongation when assembled by C6PS in solution (~ 5.8 Å) and when assembled on PS-containing membranes (R ~ 5.6 Å, Table 2). This is consistent with the report that C6PS and membranes in conjunction with FVa$_2$ elicit nearly identical functional changes [11,30]. It seems that, while C6PS and membranes may not act identically in regulating FXa structure and activity, in the presence of FVa$_2$, they have similar effects. However additional FRET distances and more complete structural studies are required to further test this hypothesis.

It is well known that prothrombin activation can occur *via* two intermediates, MzIIa (cleave at R320) or Pre2 (cleave at R271), or can occur without the release of an intermediate (channeling) [33–35]. Activation *via* MzIIa has generally been reported in the presence of synthetic PS-containing membranes. It is recently reported that prothrombin activation proceeds *via* Pre2 rather than MzIIa in the presence of platelet preparations [36]. Based on these observations, it is tempting to speculate that the conformations of enzyme, cofactor, or substrate on these different membranes might be different. Both FVa and PS-containing model membranes promote the channeling activation pathway, although the extent to which they do depends on experimental conditions (membrane, FVa, FXa concentrations) [35]. FVa is most critical to promoting the chanelling mechanism over a broad range of membranes conditions [35] and promotes chanelling even in the absence of membranes [37]. Beause experimental conditions are important in promotion channeling *versus* MzIIa release, we can not compare results obtained under very different experimental conditions to conclude that FXa assumes different conformations on platelet-derived *versus* model membranes. However, our results make clear that binding to FVa, both on a membrane and in solution, produces substantial and similar conformational changes in FXa, making it likely that the influence of FVa on prothrombin activation pathway is related to these conformational changes.

Comparison to Literature

In solution, we estimate the length of FXa to be ~ 78 – 81 Å from the active site fluorescein acceptor to the N-terminal Alexa fluor 555 donor (Tables 1 and 2). The most reliable

atomistic model we have [17] estimates the distance between the active site Ser and the N-terminus to be 83 Å. We do not wish to over interpret this agreement, but we take it mean that the atomistic model of Venkateswarlu *et al.* provides a reasonable reference point for thinking about FXa in solution.

A previous FRET study reported that that the distance from a dansyl probe linked to the active-site blocking peptide EGR a PS-containing membrane surface was 61 Å and increased by ~ 8 Å upon binding of FVa to FXa [18]. However, another paper from these researchers used a fluorescein attached to the active-site blocking peptide FPR and found this to be 84 Å from a membrane-located probe [19]. This group attributed this difference to different orientations of the EGR and FPR peptides in the active site [19], although it could also reflect the different sizes and electronic structures of the dansyl and fluorescein probes. Another paper reported that the distance from fluorescein attached to the FPR peptide to a membrane-located probe increased from 72 Å to 75 Å upon binding of FVa [20]. Our results show that FXa elongates by 4.6 Å from 79 Å upon binding FVa_2 on a membrane. However, we used fluorescein attached to the EGR peptide and measure the distance from the active site to a location that, based on our current understanding of Gla domain binding to PS-containing membranes [22], should be at the Ca^{2+} plane in the lipid phosphate plane, or at least 5–8 Å below the level of head-group-bound fluorescent probes. Based on this, our results compare best with measurements made with fluorescein attached to the FPR peptide [20]. However, it remains unclear whether FRET distances obtained with membrane-located probes [18–20] reflect the length the FXa molecule or the orientation of FXa on the membrane, or both. We removed this ambiguity by placing probes in two positions in FXa. We can thus conclude that FXa elongates slightly (~ 2.8 Å) relative to the best atomistic model [17] upon binding C6PS to it regulatory site. Based on locating a Lys in the FXa dimer interface, it has been argued that FXa in a membrane-associated dimer may not be well represented by the atomistic model [17] with the Ca^{2+} plane located at the membrane phosphate plane [23]. Our results support this suggestion in that the FRET distance we measure is slightly shorter in a membrane-associated dimer that in C6PS-bound FXa in solution (Tables 1 and 2).

While there is little quantitative agreement between the three published works that report FRET distances between active-site- and membrane-located probes, two agree that this distance increases upon binding of FVa. One study puts the change in active-site-to-membrane distance as being somewhat smaller (~ 4% [20]) and one much larger (~13% [18]) than the change in FXa length (~ 6%) that we unambiguously record for binding of FXa to FVa_2 in solution or on a PS-containing membrane (Tables 1 and 2). Given the difficulties noted in comparing published estimates of the membrane-to-active-site distance, there is ambiguity in trying to compare any one published result to our results. If we accept the measuremnts of Qureshi *et al.* as being in closet agreement with ours, we would conclude that FXa alters very little its alignment with the membrane surface upon binding membrane-assocaited FVa. However, if we accept the measurments of Huston *et al.*, we would conclude that FXa binds to a PS-containing membrane at a substantial angle to the membrane surface but "straightens up" upon binding to FVa_2. Additional work is required to resolve this ambiguity.

Recently, a crystal structure of a snake venom protein (*P textilis* propseutarin C) analogous to the FXa-FVa complex has appeared [38]. One might think that this would offer the perfect comparison to our measuements. However, the construct that was crystalized lacks the EGFn and Gla domains of whole FXa. It is thus impossible to glean from this structure a direct comparison to our measurents.

Acknowledgments

Abbreviation

FXa	Factor Xa
FVa	Factor Va
FVa$_2$	a glycoform of FVa that binds FXa in solution
PS	Phosphatidylserine
C6PS	dicaproyl-phosphatidylserine
DOPC	di-oleoyl-phosphatidylcholine
DOPS	di-oleoyl-phosphatidylserine
A555	Alexa fluor 555
Gla	γ-carboxyglutamic acid
EGF	epidermal growth factor
RVV-X	FX activator from Russell's viper venom
SUVs	small unilamellar vesicles
FRET	fluorescence resonance energy transfer
E$_{FRET}$	efficiency of energy transfer
F$_D$	fluorescence intensity of donor-labeled FXa
F$_A$	fluorescence intensity of acceptor-labeled FXa
F$_{DA}$	fluorescence intensity of double-labeled FXa
Reg-site	regulatory site
Prot-site	putative protein recognition site
MzIIa	meizothrombin
Pre2	prethrombin 2

References

1. Fenton JW 2nd. Thrombin. Ann N Y Acad Sci. 1986; 485:5–15. [PubMed: 3551733]

2. Nesheim ME, Kettner C, Shaw E, Mann KG. Cofactor dependence of factor Xa incorporation into the prothrombinase complex. J. Biol. Chem. 1981; 256:6537–6540. [PubMed: 7240226]

3. Rosing J, Tans G, Govers-Riemslag J, Zwaal R, Hemker H. The role of phospholipids and factor Va in the prothrombinase complex. J. Biol. Chem. 1980; 255:274–283. [PubMed: 7350159]

4. Bevers EM, Comfurius P, Zwaal RF. Changes in membrane phospholipid distribution during platelet activation. Biochim. Biophys. Acta. 1983; 736:57–66. [PubMed: 6418205]

5. Jones ME, Lentz BR, Dombrose FA, Sandberg H. Comparison of the abilities of synthetic and platelet-derived membranes to enhance thrombin formation. Thromb Res. 1985; 39:711–724. [PubMed: 4082107]

6. Kim SW, Ortel TL, Quinn-Allen MA, Yoo L, Worfolk L, Zhai X, Lentz BR, Kane WH. Partial glycosylation at asparagine-2181 of the second C-type domain of human factor V modulates assembly of the prothrombinase complex. Biochemistry. 1999; 38:11448–11454. [PubMed: 10471296]

7. Banerjee M, Drummond DC, Srivastava A, Daleke D, Lentz BR. Specificity of soluble phospholipid binding sites on human factor Xa. Biochemistry. 2002; 41:7751–7762. [PubMed: 12056907]

8. Banerjee M, Majumder R, Weinreb G, Wang J, Lentz BR. Role of Procoagulant Lipids in Human Prothrombin Activation. 2. Soluble Phosphatidylserine Upregulates and Directs Factor X(a) to Appropriate Peptide Bonds in Prothrombin. Biochemistry. 2002; 41:950–957. [PubMed: 11790118]

9. Koppaka V, Wang J, Banerjee M, Lentz BR. Soluble phospholipids enhance factor Xa-catalyzed prothrombin activation in solution. Biochemistry. 1996; 35:7482–7491. [PubMed: 8652526]

10. Majumder R, Quinn-Allen MA, Kane WH, Lentz BR. A phosphatidylserine binding site in factor Va C1 domain regulates both assembly and activity of the prothrombinase complex. Blood. 2008; 112:2795–2802. [PubMed: 18587009]

11. Majumder R, Weinreb G, Lentz BR. Efficient thrombin generation requires molecular phosphatidylserine, not a membrane surface. Biochemistry. 2005; 44:16998–17006. [PubMed: 16363813]

12. Srivastava A, Wang J, Majumder R, Rezaie AR, Stenflo J, Esmon CT, Lentz BR. Localization of phosphatidylserine binding sites to structural domains of factor Xa. J. Biol. Chem. 2002; 277:1855–1863. [PubMed: 11707438]

13. Wu JR, Zhou C, Majumder R, Powers DD, Weinreb G, Lentz BR. Role of Procoagulant Lipids in Human Prothrombin Activation. 1. Prothrombin Activation by Factor X(a) in the Absence of Factor V(a) and in the Absence and Presence of Membranes. Biochemistry. 2002; 41:935–949. [PubMed: 11790117]

14. Majumder R, Wang J, Lentz BR. Effects of water soluble phosphotidylserine on bovine factor Xa: functional and structural changes plus dimerization. Biophys. J. 2003; 84:1238–1251. [PubMed: 12547804]

15. Chen Q, Lentz BR. Fluorescence resonance energy transfer study of shape changes in membrane-bound bovine prothrombin and meizothrombin. Biochemistry. 1997; 36:4701–4711. [PubMed: 9109682]

16. Di Scipio RG, Hermodson MA, Yates SG, Davie EW. A comparison of human prothrombin, factor IX (Christmas factor), factor X (Stuart factor), and protein S. Biochemistry. 1977; 16:698–706. [PubMed: 836809]

17. Venkateswarlu D, Perera L, Darden T, Pedersen LG. Structure and dynamics of zymogen human blood coagulation factor X. Biophys. J. 2002; 82:1190–1206. [PubMed: 11867437]

18. Husten EJ, Esmon CT, Johnson AE. The active site of blood coagulation factor Xa. Its distance from the phospholipid surface and its conformational sensitivity to components of the prothrombinase complex. J. Biol. Chem. 1987; 262:12953–12961. [PubMed: 3477541]

19. Mutucumarana VP, Duffy EJ, Lollar P, Johnson AE. The active site of factor IXa is located far above the membrane surface and its conformation is altered upon association with factor VIIIa. A fluorescence study. J. Biol. Chem. 1992; 267:17012–17021. [PubMed: 1512240]

20. Qureshi SH, Yang L, Yegneswaran S, Rezaie AR. FRET studies with factor X mutants provide insight into the topography of the membrane-bound factor X/Xa. Biochem. J. 2007; 407:427–433. [PubMed: 17635109]

21. Lee CJ, Lin P, Chandrasekaran V, Duke RE, Everse SJ, Perera L, Pedersen LG. Proposed structural models of human factor Va and prothrombinase. J. Thromb. Haemost. 2008; 6:83–89. [PubMed: 17973648]

22. Huang M, Rigby AC, Morelli X, Grant MA, Huang G, Furie B, Seaton B, Furie BC. Structural basis of membrane binding by Gla domains of vitamin K-dependent proteins. Nat. Struct. Biol. 2003; 10:751–756. [PubMed: 12923575]

23. Chattopadhyay R, Iacob R, Sen S, Majumder R, Tomer KB, Lentz BR. Functional and structural characterization of factor Xa dimer in solution. Biophys. J. 2009; 96:974–986. [PubMed: 19186135]

24. Bock PE. Active site selective labeling of serine proteases with spectroscopic probes using thioester peptide chloromethyl ketones: demonstration of thrombin labeling using N.alpha. [(acetylthio)acetyl]-D-Phe-Pro-Arg-Ch2Cl. Biochemistry. 1988; 27:6633–6639. [PubMed: 3219359]

25. Chen PS, Toribara TY, H W. Microdetermination of phosphorus. Anal. Chem. 1956; 28:1756–1758.

26. Lakowicz, JR. Principles of Fluorescence Spectroscopy. New York: Kluwer Academic/Plenum Publisher; 1999.

27. Prazeres TJ, Fedorov A, Barbosa SP, Martinho JM, Berberan-Santos MN. Accurate determination of the limiting anisotropy of rhodamine 101. Implications for its use as a fluorescence polarization standard. J. Phys. Chem. A. 2008; 112:5034–5039. [PubMed: 18476678]

28. Zorrilla S, Rivas G, Acuna AU, Lillo MP. Protein self-association in crowded protein solutions: a time-resolved fluorescence polarization study. Protein. Sci. 2004; 13:2960–2969. [PubMed: 15459331]

29. Dale RE, Eisinger J, Blumberg WE. The orientational freedom of molecular probes. The orientation factor in intramolecular energy transfer. Biophys. J. 1979; 26:161–193. [PubMed: 262414]

30. Majumder R, Weinreb G, Zhai X, Lentz BR. Soluble Phosphatidylserine Triggers Assembly in Solution of a Prothrombin-activating Complex in the Absence of a Membrane Surface. J. Biol. Chem. 2002; 277:29765–29773. [PubMed: 12045194]

31. Koklic T, Majumder R, Weinreb GE, Lentz BR. Factor XA binding to phosphatidylserine-containing membranes produces an inactive membrane-bound dimer. Biophys. J. 2009; 97:2232–2241. [PubMed: 19843455]

32. Majumder R, Koklic T, Rezaie AR, Lentz BR. Phosphatidylserine-induced factor Xa dimerization and binding to factor Va are competing processes in solution. Biochemistry. 2013; 52:143–151. [PubMed: 23214401]

33. Nesheim ME, Mann KG. The kinetics and cofactor dependence of the two cleavages involved in prothrombin activation. J. Biol. Chem. 1983; 258:5386–5391.. [PubMed: 6687890]

34. Boskovic DS, Bajzar LS, Nesheim ME. Channeling during prothrombin activation. J. Biol. Chem. 2001; 276:28686–28693. [PubMed: 11384970]

35. Weinreb GE, Mukhopadhyay K, Majumder R, Lentz BR. Cooperative roles of factor V(a) and phosphatidylserine-containing membranes as cofactors in prothrombin activation. J. Biol. Chem. 2003; 278:5679–5684. [PubMed: 12438309]

36. Wood JP, Silveira JR, Maille NM, Haynes LM, Tracy PB. Prothrombin activation on the activated platelet surface optimizes expression of procoagulant activity. Blood. 2011; 117:1710–1718. [PubMed: 21131592]

37. Boskovic DS, Giles AR, Nesheim ME. Studies of the role of factor Va in the factor Xa-catalyzed activation of prothrombin, fragment 1.2-prethrombin-2, and dansyl-L-glutamyl-glycyl-L-arginine-meizothrombin in the absence of phospholipid. J. Biol. Chem. 1990; 265:10497–10505. [PubMed: 2355010]

38. Lechtenberg BC, Murray-Rust TA, Johnson DJ, Adams TE, Krishnaswamy S, Camire RM, Huntington JA. Crystal structure of the prothrombinase complex from the venom of Pseudonaja textilis. Blood. 2013; 122:2777–2783. [PubMed: 23869089]
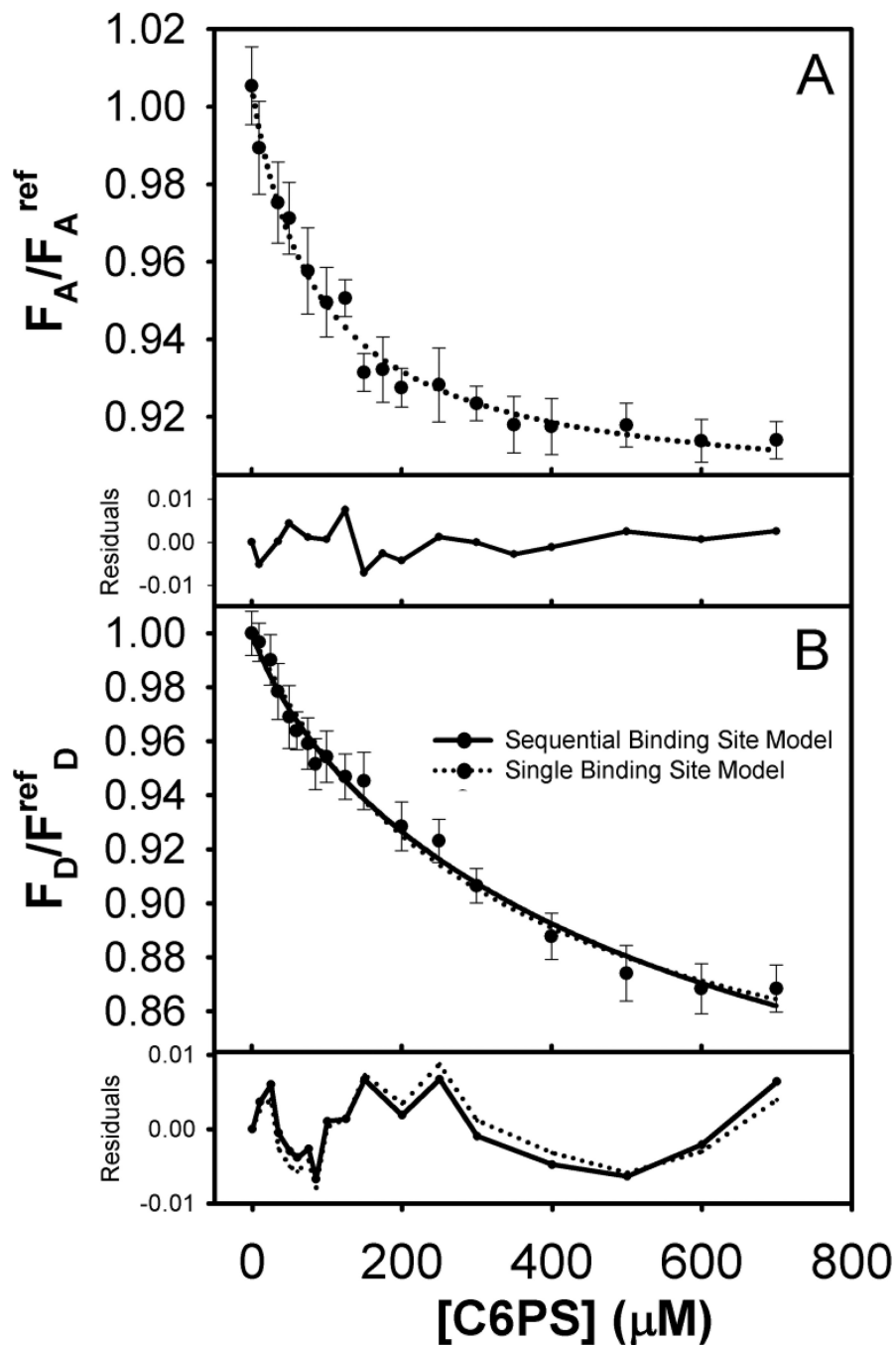
Figure 1.

(A) Fluorescence intensity of *acceptor*-labeled FXa (15 nM) in Tris buffer (50 mM Tris, 150 mM NaCl, 5 mM CaCl2, 0.6% PEG, 7.4 pH) upon titration with C6PS at 23°C. Observed intensities were normalized against the intensity of an Alexa fluor 555 reference solution. Symbols represent an average value with standard deviations as error bars. The dotted curve drawn through the symbols show a fit of the data to a single-site binding model which gives k_{d1}=73 μM. **(B)** Fluorescence intensity of *donor* labeled FXa (15 nM) upon titration with C6PS at 23°C. Observed intensities were normalized against the intensity of a fluorescein

reference solution. Symbols and error bars are as in Frame A, as is the dotted curve that shows a fit of the data to a single-site binding model with k_{d1}=333 μM. The solid curve drawn through the symbols shows a fit to a sequential-linked-site model wherein we fixed the first binding site k_{d1} at 73 μM, resulting in the second binding site constant k_{d2} being 714 μM. The frames below frames A and B show the residuals for each predicted curve compared to experimental values.
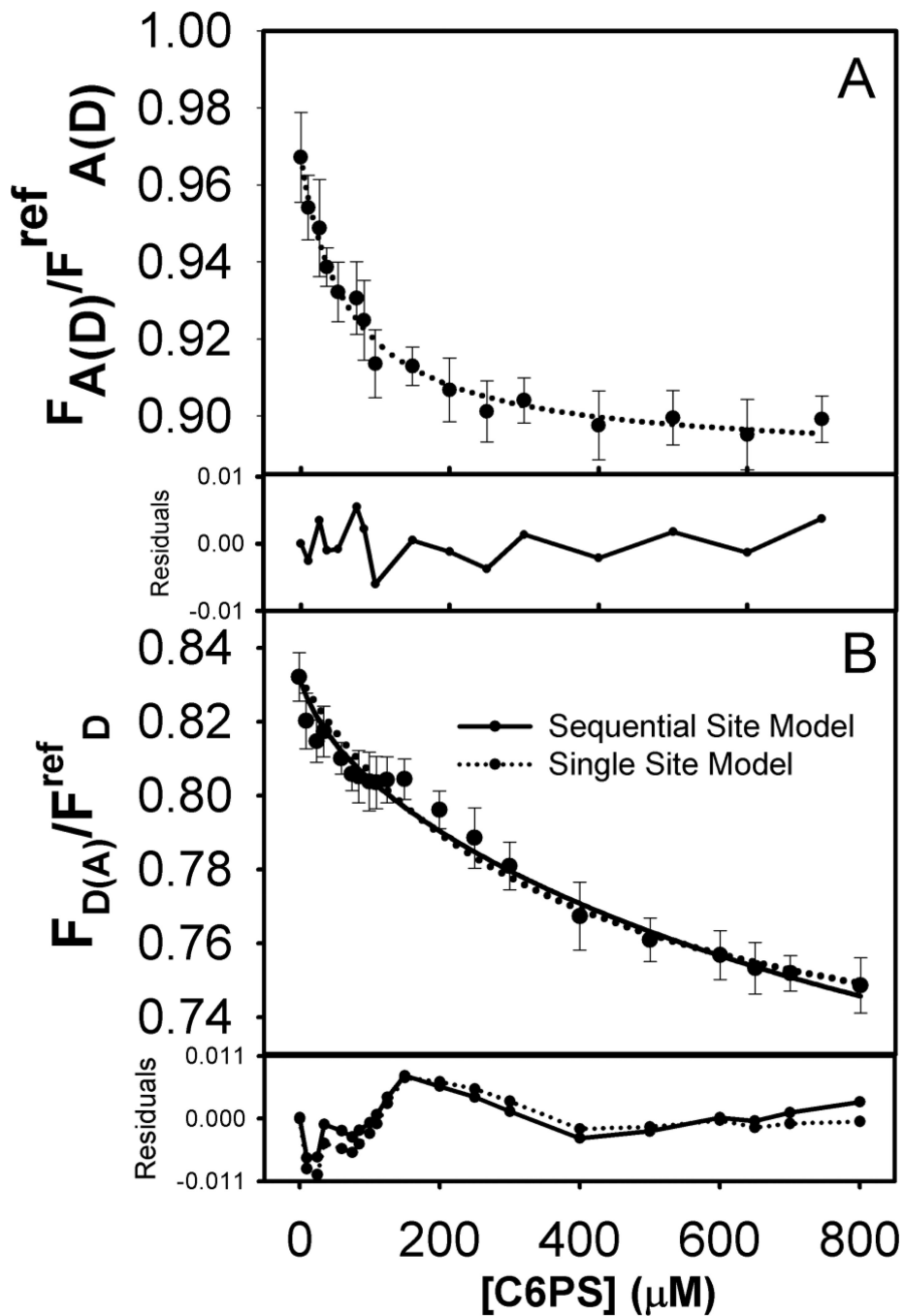
Figure 2.
(A) Normalized fluorescence intensity of *acceptor* in double labeled FXa (15 nM) upon titration with C6PS at 23°C, with details as described in Figure 1. Again, the dotted curve shows a fit of the data to a single-site binding model with k_{d1}=76 μM. **(B)** Normalized fluorescence of *donor* in double labeled FXa (15 nM) upon titration with C6PS at 23°C. As in Figure 1, the dotted curve shows a fit of the data to a single-site binding model with k_{d1}=370 μM, while the solid curve shows a fit with a sequential-linked-site model with the

first binding site constant k_{d1}=50 μM and an adjusted second binding site constant k_{d1}=1000 μM. Residual plots are shown below each frame.
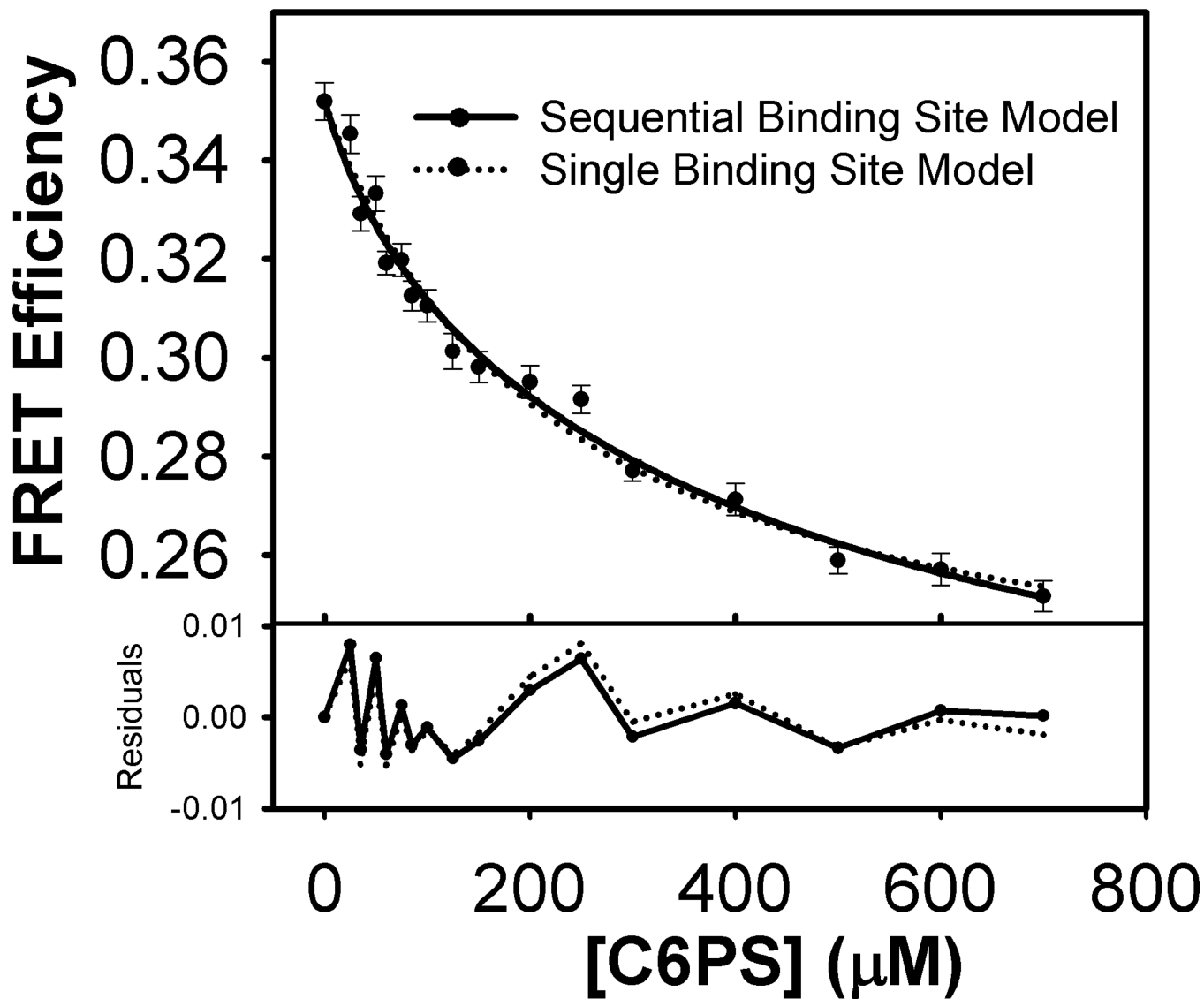
Figure 3.
Variation of FRET efficiency with C6PS concentration obtained from the data in Figures 2B and 3B using Equation 1 in Material and Methods.
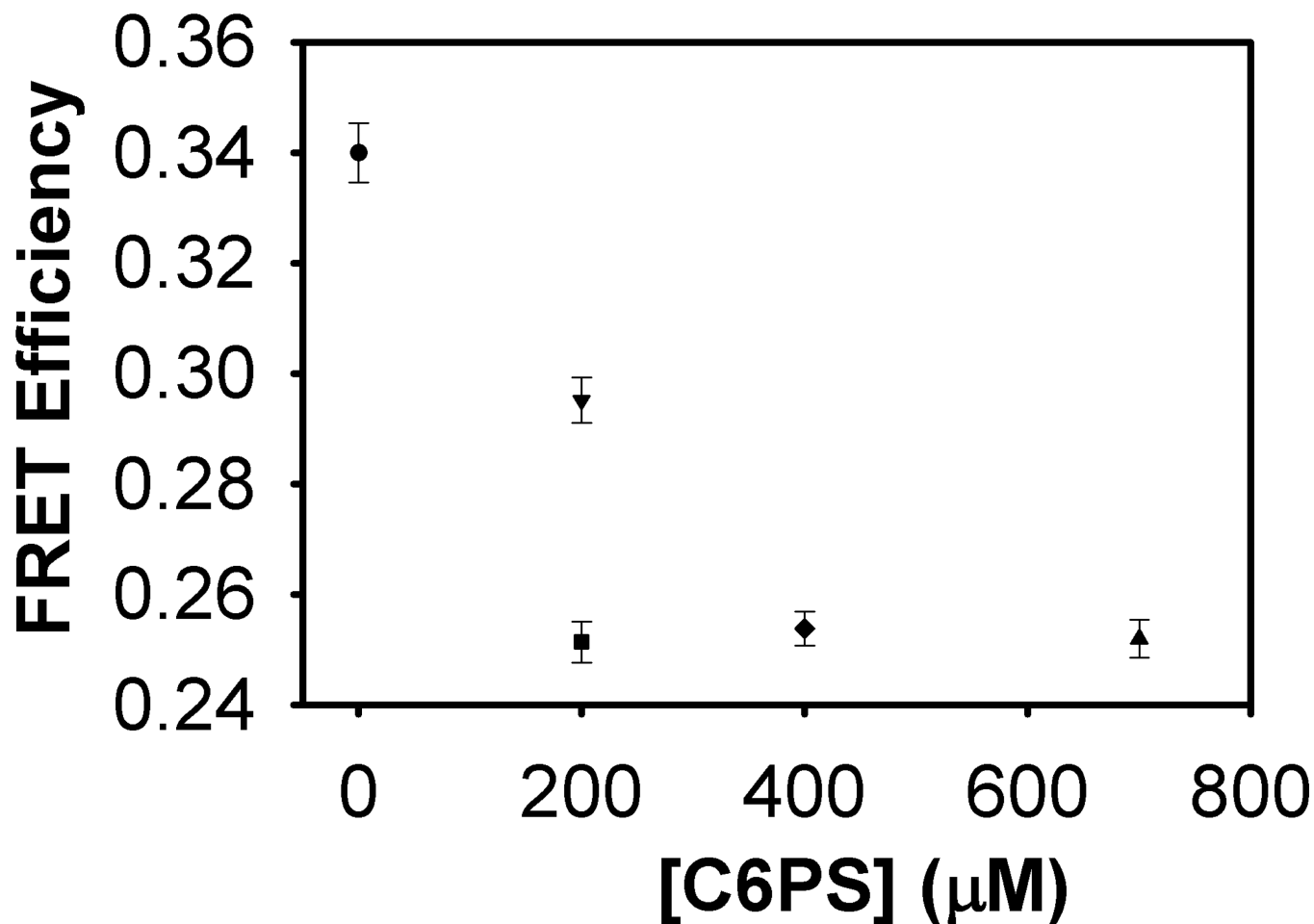
Figure 4.
FRET efficiency as a function of C6PS binding in the presence of FVa$_2$. FRET efficiency values were calculated from fluorescence intensity data of F$_D$ and F$_{D(A)}$ using equation 1 mentioned in Materials and Methods. Average FRET efficiency values on each addition of either C6PS or FVa$_2$ are presented as symbols along with their standard deviations as error bars. FRET efficiency of FXa (in 1:9 ratio of labeled: unlabeled FXa) (circle), followed by addition of 200 μM C6PS (downward triangle), followed by addition of FVa$_2$ (square), then increases in total C6PS to 400 μM (diamond) and to 700 μM (upward triangle).
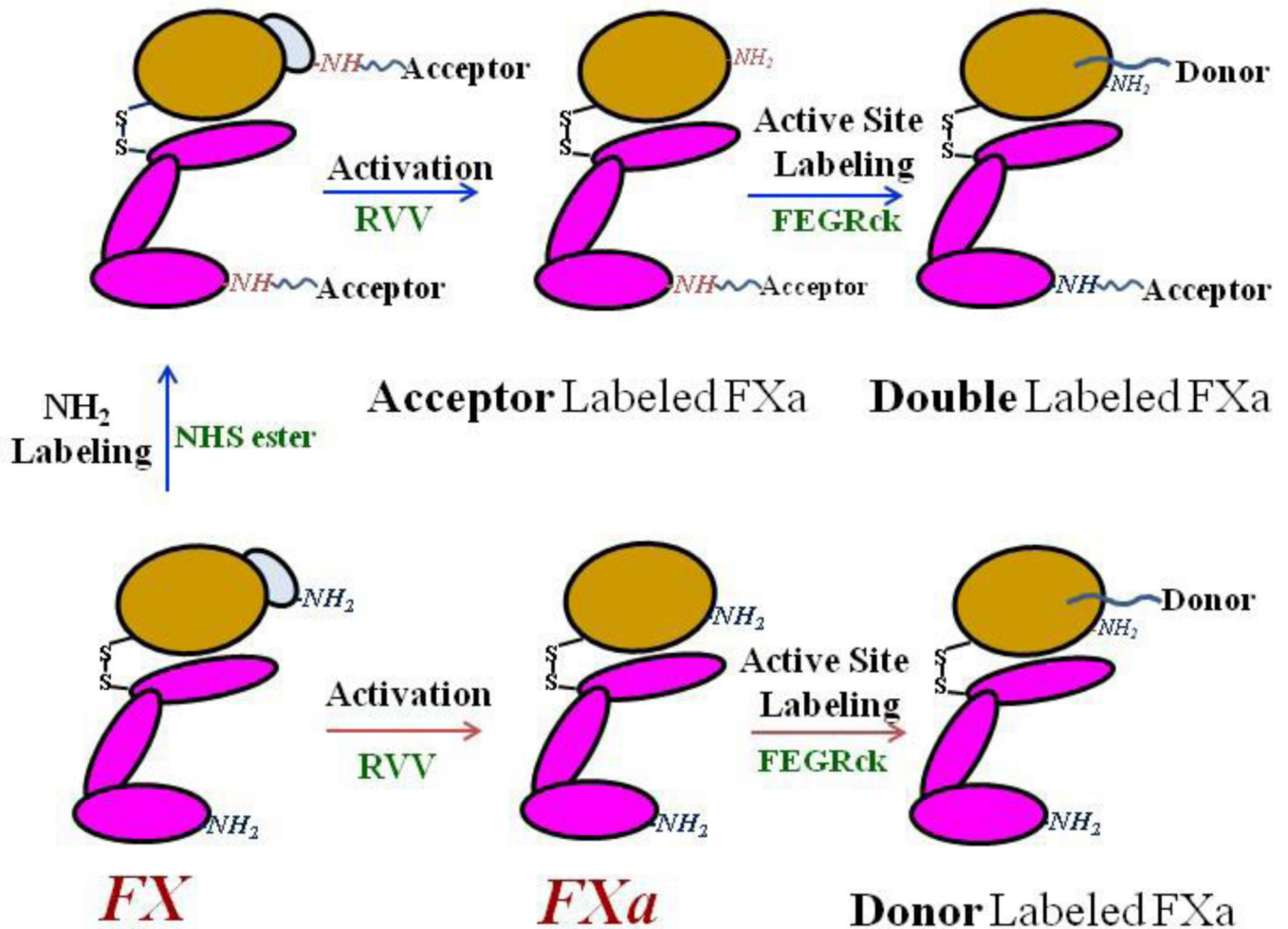
Scheme 1.
Schematic representation of preparation of fluorophore-labeled FXa. FX was first labeled
with donor (Alexa Fluor 555 succinimidyl ester; A555-NHS) followed by activation to
remove the activation peptide at its N-terminus. The acceptor (fluorescein-labeled EGR-
chloromethylketone; FEGRck) was then added to the active site of A555-Xa to produce
doubly labeled peptide or to FXa to produce singly labeled peptide.

NIH-PA Author Manuscript   NIH-PA Author Manuscript   NIH-PA Author Manuscript

Table 1

The calculated FRET efficiency values and corresponding calculated distances between covalently attached fluorophore. The distances were calculated assuming random dipolar orientation ($\kappa^2=2/3$) of fluorophores as described in experimental procedure. The range of κ^2 was calculated from anisotropy values of donor and acceptor and then distances were corrected for the range of κ^2 [29].

C6PS Concentration	E_{fret}	Distance (Å) with $\kappa^2=2/3$	κ^2	κ^2-corrected Distance (Å)	
				range	mean
Initial (no C6PS)	0.340 ± 0.004	78.1 ± 0.34	$0.19 - 2.60$	$63.3 - 98.4$	80.8 ± 17
First Site Saturation	0.295 ± 0.003	80.9 ± 0.33	$0.17 - 2.76$	$64.3 - 102.2$	83.3 ± 19
700 µM	0.252 ± 0.003	83.9 ± 0.48	$0.14 - 2.98$	$64.6 - 107.4$	86.0 ± 21
Complete Saturation	0.2074	87.5 ± 0.39	$0.14 - 2.98$	$67.2 - 112.5$	89.8 ± 22

Table 2

The observed anisotropy values of fluorescein (donor), calculated FRET efficiency (E_{fret}) values and corresponding calculated distances between covalently attached fluorophores assuming random dipolar orientation ($\kappa^2=2/3$). FRET efficiency values for each addition of SUV, C6PS and FVa were calculated from fluorescence intensity data of F_D and $F_{D(A)}$ using equation 1 mentioned in Materials and Methods. The error value of E_{fret} was calculated from the sum of fractional error of observed F_D and F_{DA}.

	Anisotropy	E_{fret}	Distance (Å)
FXa	0.17 ± 0.003	0.344 ± 0.003	77.9 ± 0.26
FXa-Membrane	0.17 ± 0.002	0.320 ± 0.004	79.3 ± 0.34
FXa-Membrane-FVa	0.22 ± 0.003	0.277 ± 0.004	83.9 ± 0.33
FXa	0.17 ± 0.003	0.340 ± 0.004	78.1 ± 0.34
FXa-200µMC6PS	0.18 ± 0.005	0.295 ± 0.003	80.9 ± 0.35
FXa-200µMC6PS-FVa	0.21 ± 0.003	0.251 ± 0.003	83.9 ± 0.34
FXa-400µMC6PS-FVa	0.22 ± 0.002	0.254 ± 0.003	83.8 ± 0.27
FXa-700µMC6PS-FVa	0.22 ± 0.002	0.252 ± 0.003	83.9 ± 0.31